RSC Advances

ROYAL SOCIETY OF CHEMISTRY

www.rsc.org/advances

Cite this: DOI: 10.1039/c0xx00000x

www.rsc.org/xxxxxx

ARTICLE TYPE

Biodegradable polylactide based materials with improved crystallinity, mechanical properties and rheological behaviour by introducing long-chain branched copolymer

Ming-Jing Liu, Si-Chong Chen*, Ke-Ke Yang*, Yu-Zhong Wang

Received (in XXX, XXX) Xth XXXXXXXXX 20XX, Accepted Xth XXXXXXXXX 20XX
DOI: 10.1039/b000000x

Herein we developed a novel strategy for preparing biodegradable polylactide (PLA) based materials with improved crystallinity, mechanical properties and rheological behaviour by introducing long-chain branched block copolymer (LB-PCLA) of PLA and poly-ε-caprolactone (PCL). The LB-PCLA copolymer was synthesized by single hydroxyl-terminated PLA (PLA-OH) and three hydroxyl-terminated PCL (PCL-3OH) precursors. The crystallinity and crystal morphology of PLA/LB-PCLA blends were investigated by differential scanning calorimetry (DSC) instrument and polarized optical microscopy (POM). The morphology and domain size of PLA/LB-PCLA blends were investigated by transmission electron microscopy (TEM). The irregular dispersed droplets shape of LB-PCLA copolymer suggested that the interfacial interaction between the PLA and PCL phases was obviously compatibilized because of the copolymerization and the branched structure of the LB-PCLA. This phase morphology is responsible for the enhancement in crystallinity, crystallization rate, and toughness of the PLA/LB-PCLA blends comparing to neat PLA and PLA/PCL blends. The elongation at break for PLA/LB-PCLA blend with 15wt% of the LB-PCLA copolymer was about 210%, an increase of 30 times compared with that of neat PLA. Rheological behaviour also shows that the LB-PCLA copolymer and PLA/LB-PCLA-15 has more pronounced shear thinning behaviour and longer relaxation time than neat PLA and PLA/PCL blend with 15wt% of the PCL, which can be attributed to the long-chain branched structure of LB-PCLA copolymer.

Introduction

Polylactide (PLA) is a thermoplastic aliphatic polyester which can be produced from annually renewable resources. It has a number of excellent properties including biodegradability, biocompatibility, good mechanical properties and processability, and has widely been used in biomedical materials and general plastics.[1-3] However, the broad applications of PLA as a commodity polymer have been restricted significantly by its inherent brittleness and poor melt rheological behaviour. The toughening of PLA has been studied for a long time and different approaches have been used to improve it.[4-10] Some studies have focused on polycondensation and chain extension methods to toughen PLA, but the brittleness of PLA is not prominently changed due to the inherent chemical structure.[11] Chemical copolymerization with other flexible polymer is an efficient way to toughen PLA, but the other excellent properties of PLA were also influenced.[12] Physical blending provides an economic solution to modify the properties of PLA. Polymers with good toughness, such as poly-ε-caprolactone (PCL),[13] polyethylene glycol (PEG),[14] hyperbranched polymer (HBP),[15] crosslinked polyurethane (CPU)[16] were used as toughening agents for PLA. The enhancement is not very obvious since the phase separation occurred in the absence of compatibilizers. It destroyed the mechanical properties dramatically.[17-19] As a semi-crystalline polymer, the physical as well as mechanical properties of PLA can be significantly affected by the crystallization characteristics. The introduction of heterogenetic polymer toughening agent by blending may inevitably decrease the crystallization properties of the PLA because of the incompatibility. The microstructure of blends has very important influence on the crystallization and mechanical properties of bulk PLA.[20-26]

Melt rheological behaviour is another important issue that should be addressed for the application of PLA based materials.[27-31] Introducing long-chain branched (LB) structure to linear polymer is an effective approach to improve the melt rheological behaviour owing to the enough entangling with other chains in melt.[32-35] LB polymers are found to exhibit the following properties: the zero shear viscosity is higher and shear thinning is stronger than linear polymers of equal molecular weight, which is advantageous for certain processing operations. It has strong melt elasticity, storage modulus and enhanced strain hardening under elongational flow.[36-37] Various types of long-chain branched polyesters such as comb-like, star-branched, super-branched and randomly branched polyesters, were prepared using different polymerization techniques.[35]

With growing environmental and energy problems, finding a complete environmental-benign and biodegradable blend polymer

component completely renewable blending to enhance PLA properties remains a challenge.[38-43] The aim of this work is to develop a comprehensive solution strategy to toughen PLA without obvious injuring other properties such as crystallization and rheological behaviour. Thus, the long-chain branched block copolymer (LB-PCLA) was prepared and blended with neat PLA. The interfacial interaction between PCL and PLA segments was effectively compatibilized when LB-PCLA copolymer was added. Moreover, the long-chain branched structure can also improve the melt rheological behaviour and processing properties of bulk PLA.

Experimental

Reagents and materials

The ε-caprolactone (CL) monomer which was provided by J&K Chemical was purified by vacuum distillation over CaH_2. $Sn(Oct)_2$ which was received from Sigma Chemical was diluted with anhydrous toluene. Trimethylolpropane (TMP), benzyl alcohol (BnOH) and ethyl acetate (EA) were purchased from Sinopharm Chemical Reagent Co, Ltd. TMP was used after recrystallization from EA. L-Lactide was purchased from Jinan Daigang Biomaterial Co, Ltd (Shandong, China) without further purification. PLA 4032D was provided by NatureWorks LLC. The molecular weight (M_w) and distribution (PDI) of PLA are 1.3×10^5 g mol^{-1} and 2.9, respectively. Poly-ε-caprolactone (PCL) was provided by Jinan Daigang Biomaterial Co, Ltd. The molecular weight (M_w) and distribution (PDI) of PCL are 1.5×10^5 g mol^{-1} and 2.2, respectively. Hexamethylene diisocyanate (HDI) was purchased from Tokyo Chemical Industry Co. All other reagents were analytical grade and used without further purification.

Synthesis of LB-PCLA copolymer

The preparation of LB-PCLA copolymer followed the outline in previous research.[44-46] Scheme 1 shows the synthesis route of LB-PCLA copolymer. Typically, a certain amount of ε-caprolactone as the monomer and trimethylolpropane (TMP) with three hydroxyl groups as initiator, were placed in a previously flame-dried and nitrogen purged flask equipped with a stirrer. The polymerization was then conducted at 120 °C for 48 h under nitrogen atmosphere using $Sn(Oct)_2$ as catalyst to obtain the three-hydroxyl-terminated PCL precursor (PCL-3OH). Single hydroxyl-terminated PLA-OH precursor was synthesized by ring opening polymerization as follows: a certain amount of L-Lactide and benzyl alcohol (BnOH) were placed in a round-bottomed flask and $Sn(Oct)_2$ was added as catalyst. The mixture was heated in an oil bath at 130 °C for 24 h in a nitrogen atmosphere. The average molecular weights of PLA-OH and PCL-3OH precursors used in this work were 2.0×10^3 and 6.1×10^3 g mol^{-1} calculated from ^{1}H NMR measurement, respectively. Purified PCL-3OH and PLA-OH precursors were then copolymerized using HDI as the coupling agent. The LB-PCLA copolymer was dissolved in chloroform and precipitated by methanol so as to remove smaller molecules. The weight fraction of PLA segments in the copolymer was 53% calculated by ^{1}H NMR measurement. The molecular weight and distribution measurements were performed using a Waters GPC device equipped with a 1515 pump, a Waters model 717 auto sampler, and a 2414 refractive index detector. Chloroform was used as the eluent with flow rate 1.0 ml min^{-1}. A calibration curve was obtained using mono-disperse polystyrene standards.

The average molecular weight and distribution of PLA-OH and PCL-3OH precursors and the LB-PCLA copolymer obtained from GPC were shown in Fig. 1. The elution time of LB-PCLA copolymer significantly reduced compared with PLA-OH and PCL-3OH precursors, and all tested samples showed single peak, no other small peaks. The results clearly showed that PLA-OH, PCL-3OH precursors and LB-PCLA copolymer were synthesized successfully.

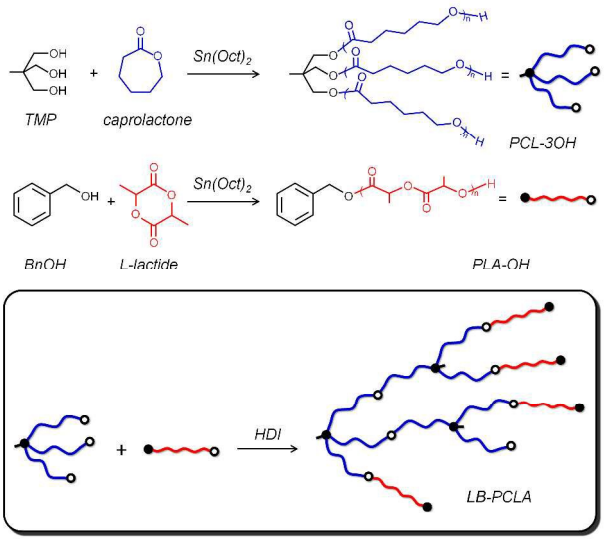

Scheme 1 Synthesis route of LB-PCLA copolymer.

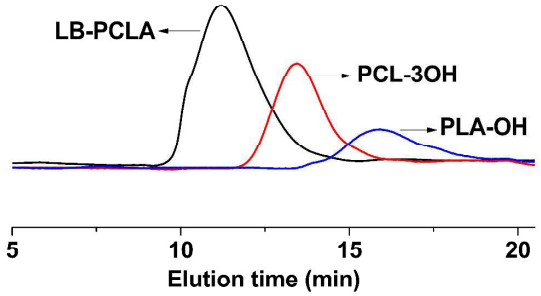

Fig. 1 GPC traces of PLA-OH, PCL-3OH precursors and LB-PCLA copolymer

The ^{1}H NMR ($CDCl_3$, 400 MHz) spectra for PLA-OH, PCL-3OH and LB-PCLA were shown in the following data. The typical resonances signals suggesting that the precursors and copolymer were successfully synthesized.

(a) PLA-OH precursor: ^{1}H-NMR (400 MHz, $CDCl_3$, δ): 5.18 (m, H, -O-C***H***CH_3CO-), 4.36 (m, H, -C***H***CH_3OH), 1.58 (d, 3H, -O-CHC***H***$_3$CO-).

(b) PCL-3OH precursor: ^{1}H-NMR (400 MHz, $CDCl_3$, δ): 1.62 (m, 4H, -C***H***$_2$-CH_2-C***H***$_2$-CH_2-O-), 1.35 (m, 4H, -CH_2-C***H***$_2$-CH_2-CH_2-O-), 2.32 (t, 2H, -CO-C***H***$_2$-), 4.06 (t, 2H, -CH_2-CH_2-CH_2-C***H***$_2$-O-), 0.88 (t, 3H, C***H***$_3$-CH_2-C-(CH_2-O-)$_3$), 1.41 (m, 2H, CH_3-C***H***$_2$-C-(CH_2-O-)$_3$), 4.1 (s, 2H, CH_3-CH_2-C-(C***H***$_2$-O-)$_3$).

(c) LB-PCLA copolymer: ^{1}H-NMR (400 MHz, DMSO-d_6, δ): Besides typical resonances signals of the two precursors, 7.18 (t,

2H, -CON***H***$CH_2CH_2CH_2CH_2CH_2CH_2N$***H***CO-), 2.98 (t, 4H,-NH C***H***$_2CH_2CH_2$ CH_2CH_2C***H***$_2$NH), 1.43 (m, 4H, -$CONHCH_2C$***H***$_2$ CH_2CH_2C***H***$_2CH_2NHCO$), 1.26 (m, 4H, -$CONHCH_2CH_2C$***H***$_2C$***H***$_2$ CH_2CH_2NHCO-).

Preparation of PLA/LB-PCLA blends

The PLA/LB-PCLA blends were prepared by melt blending. Before processing, PLA was dried at 80 °C in a vacuum oven for 24 h. The melt blends were prepared using a Haake batch intensive mixer (Haake Rheomix 600, Karlsruhe, Germany) with a batch volume of 50 mL at 190 °C and a screw speed of 50 rpm during a total mixing time of 5 min. The blends were taken out to cool down to room temperature slowly before testing. The resulting samples were identified as PLA/LB-PCLA-15, PLA/LB-PCLA-25, PLA/LB-PCLA-35, PLA/LB-PCLA-45 and LB-PCLA denotes the long-chain branched copolymer, the number after it refers to its mass percentage. To compare with PLA/LB-PCLA blends, PLA/PCL blends with the same content were also discussed.

Differential scanning calorimetry measurement (DSC)

The resulting blends of approximately 5 mg in weight were encapsulated in aluminum pans and measured in a DSC (Q200, New Castle, DE) instrument under nitrogen atmosphere. PLA exhibits a T_g at approximately the same temperature as the T_m of PCL, PLA cold crystallizes around 100 °C, and PLA melts around 170 °C. In the non-isothermal experiment, the samples were first fast heated to 190 °C for 3 min to erase all previous thermal history. Then, the samples were cooled to -90 °C, after that, the samples were second heated by 10 °C min^{-1} to 190 °C. In the isothermal crystallization, the samples were again heated to 190 °C, then cooled to 115 °C rapidly and kept for enough time to let the PLA segments in the samples crystallize completely.

Wide-angle X-ray diffraction (WAXD)

Wide-angle X-ray diffraction (WAXD) was performed at RT using a Rigaku D/Max 2500V PC X-ray diffractometer (Japan). The CuKα radiation (λ=0.15418 nm) source was operated at 40 kV and 200 mA. Measurements were recorded in the 2θ range 5-35 ^{o} at a scanning speed of 4 ^{o} min^{-1}.

Polarized optical microscopy (POM)

The crystal morphology of samples at different crystallization temperatures was studied with a Nikon ECLIPSE LV100POL microscope in conjunction with a hot stage (HSC621V). Photographs were taken by a digital camera. The samples for the polarized optical microscopy (POM) test were prepared as follows: all samples were first dissolved in chloroform ($CHCl_3$) with a concentration of 10 mg mL^{-1}. Then, 0.05 ml solution was dripped on a glass slide and heated to 190 °C to evaporate the $CHCl_3$.

Dynamic mechanical analysis (DMA)

Thermo-mechanical properties of the blending sheets obtained by the compression-molding were tested in the solid state with a dynamic mechanical analyzer (DMA Q800, TA Instruments, USA) in a tensile mode. Tests were performed from -90 °C to 120 °C at a heating rate of 3 °C min^{-1} and an oscillation frequency of 1 Hz.

Transmission electron microscopy (TEM)

The morphology and size of dispersed phase were studied by transmission electron microscopy (TEM, Tecnai G2F20 S-TWIN electron microscope, FEI, Holland) using stained ultrathin sections at an accelerated voltage of 200 kV. Ultrathin sections of 70-80 nm in thickness were sliced using a RMC cryoultramicrotome equipped with a diamond knife. Osmium tetroxide (OsO_4) vapour was used to selectively stain the dispersed LB-PCLA phase for 25 min.

We calculated the particles by Image J analysis software. The weight-average particle diameter (d_w) using the following equation [47]:

$$d_w = \frac{\sum n_i d_i^2}{\sum n_i d_i} \quad (1)$$

Where n_i is the number of particles having diameter d_i. At least 100 particles from independent TEM images were analysed to calculate weight-average particle diameter (d_w) using the following equation. The cross-sectional area (Ai) of each individual particle (i) was measured and converted into an equivalent diameter of a sphere by the equation di = $(4Ai/\pi)^{0.5}$. Additionally, particles whose domain sizes were too small to be properly measured at the magnification chosen were neglected.

Mechanical properties measurements

All samples were preconditioned in 50% relative humidity (RH) at 25 °C for 48 h before testing. The tensile strength and elongation at break of the samples were measured on an Instron Universal Testing Machine (Model 4302, Instron Engineering Corporation, Canton, MA) at a crosshead speed of 5 mm min^{-1}. The testing temperature and RH were 25 °C and 50%, respectively. Each sample was measured at least five times to take the average.

Scanning electron microscopy (SEM)

The morphology of the fractured surfaces which were sputter-coated with a thin layer of gold prior was examined by scanning electron microscopy (JSM-5900LV, JEOL) at an accelerating voltage of 5 kV.

Melt rheological behaviour measurement

The rheological measurements were undertaken using a Bohlin Gemini 200 instrument (Malvern, UK) with 25-mm diameter parallel-plate geometry at 190 °C. The test samples were pressed into 1-mm-thick plates. Dynamic oscillatory shear measurements were performed when the angular frequency (ω) range and strain used during testing were 0.01-100 rad/s and 1%, respectively.

Results and discussion

Crystallization property of PLA/LB-PCLA blends

The non-isothermal crystallization and isothermal crystallization kinetics of PLA segments within the PLA/LB-PCLA blends were investigated by DSC. Fig. 2 showed the second heating scan from -90 °C to 190 °C after erase thermal history at 190 °C for 3 min. It can be seen that the neat PLA exhibited a broad and indistinct exothermic peak during heating. The crystallization temperatures range of neat PLA was 104-132 °C, suggested that the crystallization of neat PLA was very weak. With increase of LB-

PCLA content, the glass transition peak of PLA was gradually overlapped by the melting peak of PCL segments in the DSC curves. Table 1 showed the detailed data. The crystallization temperatures associated with the PLA segments for all the studied blends gradually shifted to higher temperature region with increasing LB-PCLA content, which were also significantly lower than that of neat PLA. This phenomenon indicated that the PLA segments of PLA/LB-PCLA blends crystallized more readily than neat PLA, and the cold crystallization ability of PLA was enhanced by LB-PCLA copolymer. Especially for PLA/LB-PCLA-15, the enhancement is largest. The relative crystallinity χ_c of PLA segments for the second heating scan was calculated using the following equations:

$$x_c = \frac{\Delta H_m}{\Delta H_m{}^0 \times \mathrm{PLA(wt\%)}} \times 100\% \quad (2)$$

Where $\Delta H_m{}^0$ is the melting enthalpy per gram of PLA in its completely crystalline state (93 J g^{-1}), PLA (wt%) is the content of the PLA segments in weight fraction which included PLA segments both in neat PLA and LB-PCLA copolymer (The weight fraction of PLA segments in the copolymer was 53% calculated by ^{1}H NMR measurement).

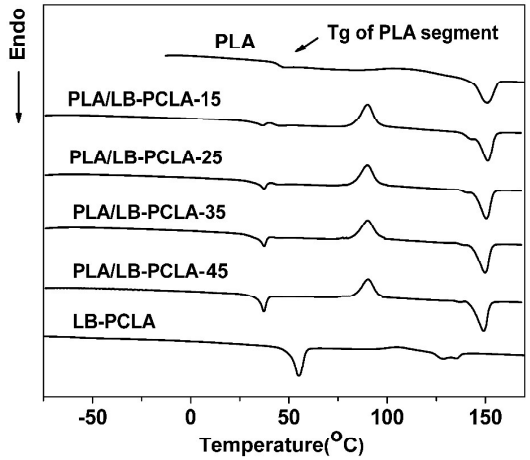

Fig. 2 The second heating scan of DSC for PLA/LB-PCLA blends after erase thermal history.

The relative crystallinity of PLA/LB-PCLA was obviously higher than neat PLA. PLA segments crystallized at the temperature higher than the melting point of the PCL segments. Since the PLA segments of LB-PCLA copolymers are chemically bonded with melted PCL segments and have relatively short chain length, they may have relatively high chain mobility and therefore enhanced the crystallization ability of PLA in the blends by reducing the energy required during crystallization for the chain folding process. Those PCL segments of LB-PCLA copolymer, which were chemically bonded with PLA, may increase the mobility of molecular chain and the crystallization ability of the PLA segments. However, for LB-PCLA, the relative crystallinity of PLA segment was smaller than those of PLA/LB-PCLA blends. This phenomenon could be attributed to the high branched content of this sample. The chain entanglements may inevitably depress the chain mobility as well as the crystallization of LB-PCLA.

Table 1 DSC thermal characteristics obtained from the second heating scan of PLA/LB-PCLA blends.

samples	T_g (°C)	T_c (°C)	T_m (°C)	ΔH_m (J/g)	χ_c (%)
PLA	62	104-132	168	22	23
PLA/LB-PCLA-15	61	98	169	30	35
PLA/LB-PCLA-25	61	99	168	28	35
PLA/LB-PCLA-35	-	99	168	26	34
PLA/LB-PCLA-45	-	99	167	25	34
LB-PCLA	-	105	128	11	23

Fig. 3 (a) showed the relationship between relative crystallinity and time for PLA segments at 115 °C for all the studied blends. The isothermal crystallization was analyzed with the classical Avrami equation.[45-46]

$$1 - \chi(t) = \exp(-kt^n) \quad (3)$$

Where n is known as the Avrami index, k is the overall rate constant including nucleation and crystal growth, and $\chi(t)$ is the relative crystallinity. We defined $t_{1/2}$ as the half-crystallization time, so that

$$1/2 = 1 - \chi(t) = \exp(-kt^n) \quad (4)$$

that is

$$t_{1/2} = \left(\frac{\ln 2}{k}\right)^{1/n} \quad (5)$$

with

$$(t_{1/2})^{-1} = \tau_{1/2} = G \quad (6)$$

Where G is defined as the crystallization rate, so $\tau_{1/2}$ directly reflects the magnitude of the crystallization rate at different crystallization temperatures. Eqn (3) could also be expressed as

$$\log\left[-\ln(1-\chi(t))\right] = \log k + n \log t \quad (7)$$

Fig. 3 (b) showed log[-ln(1-$\chi(t)$)] as a function of log t for all studied blends, where n is the slope of the straight line calculated by linear-fitting and k is the intercept. For an integrity comparison for all blends, we also performed the Avrami analysis for these samples. The values of $\tau_{1/2}$, n and k were listed in Table 2. The Avrami plots of blends had relatively low linearity owning to the interaction between PLA and PCL segments, and it resulted in deviation in the values of k and n.

It should be noted that it was not precise to discuss the overall crystallization rate directly from the k values as the unit of k is min^{-n} and n is not constant. Therefore, the $\tau_{1/2}$ was used to evaluate the crystallization kinetics.[48-49] The $\tau_{1/2}$ values of PLA segments in all blends were higher than that of neat PLA and decreased with increase of LB-PCLA copolymer content, which correlated well with the values of k. PLA/LB-PCLA-15 had the maximum $\tau_{1/2}$ value, 0.43, an increase of 10 times compared with that of neat PLA, indicated that the crystallization rate of PLA was accelerated by a small addition of LB-PCLA copolymer.

However, the crystallization rate of PLA showed a decreased trend when more copolymer was added into the blends. This result confirmed again that large amount addition of LB-PCLA copolymer gradually frustrated the crystallization of PLA.

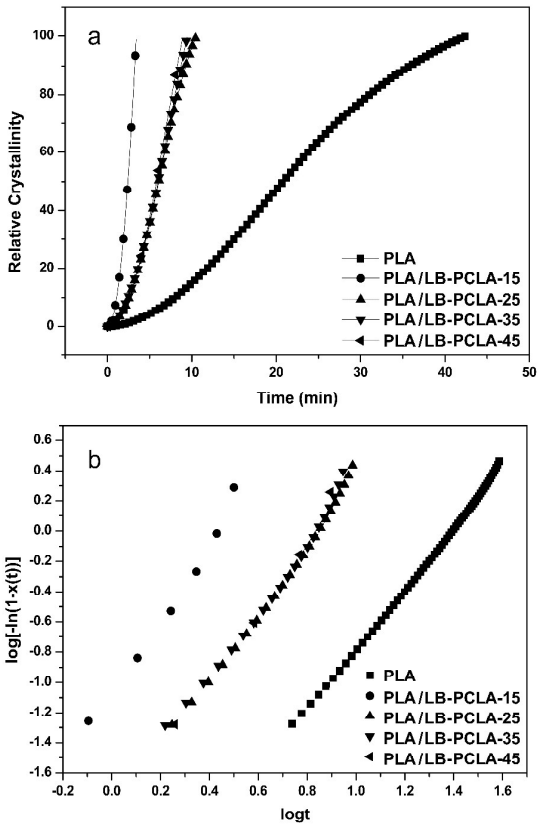

Fig. 3 (a) Extent of crystallization versus time and (b) Avrami curve for PLA/LB-PCLA blends at 115 °C respectively.

Table 2 Relevant data of isothermal crystallization and Avrami curves of PLA/LB-PCLA blends

Sample	T_c (°C)	$t_{1/2}$ (min)	$\tau_{1/2}$ (min^{-1})	n	k (min^{-n})
PLA	115	20.44	0.0489	2.04	0.00146
PLA/LB-PCLA-15	115	2.33	0.430	2.59	0.0778
PLA/LB-PCLA-25	115	5.75	0.174	2.29	0.0126
PLA/LB-PCLA-35	115	5.78	0.173	2.32	0.0114
PLA/LB-PCLA-45	115	5.81	0.172	2.48	0.00962

The crystal structure of PLA/LB-PCLA blends melt-crystallized at 115 °C and 30 °C was investigated using WAXD. The results were shown in Fig. 4. The main characteristic diffraction peaks of PLA segments in the blends are at around 14.9 °, 16.7 ° and 19.1 °, corresponding to (010), (200)/(110) and (203), respectively. These peaks are ascribed to the usual α-form of PLA. With increase of LB-PCLA content, the position of diffraction peaks showed little change. This results indicated that LB-PCLA copolymer only increased the crystallinity and did not significantly modify the crystal structure of PLA segments.[50] The main characteristic diffraction peaks of PCL segments in blends are at around 21.5 ° and 23.6 °, corresponding to (110), (200), respectively, which are ascribed to the characteristic crystal of PCL in PLA/LB-PCLA blends. With increase of LB-PCLA content, the position of PCL diffraction peaks showed little change, indicated that the crystal structure of PCL segments in the blends was also not transformed.

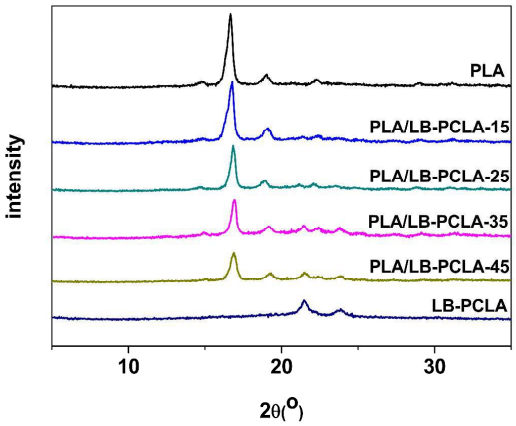

Fig. 4 WAXD patterns of PLA/LB-PCLA blends.

Crystal morphology of PLA/LB-PCLA blends

The crystal morphology of polymer blends was investigated by polarized optical microscopy (POM). The melting point (T_m) differences between PLA and PCL segments in PLA/LB-PCLA blends were over 100 °C. The crystallization of the low T_m component occurred after the complete crystallization of the high T_m component. Thus, it was very easy to distinguish the crystals of PLA and PCL segments during the crystallization of PLA/LB-PCLA blends. In consideration of the crystallization temperature of PCL and PLA segments, the POM measurement were performed as follow procedures: (1) PLA/LB-PCLA blends were directly crystallized at 30 °C or 115 °C separately after melting at 190 °C for 3 min; (2) the blends were crystallized at 30 °C after crystallization of PLA segments at 115 °C.

When PLA/LB-PCLA blends were treated at 115 °C for enough time, only PLA segments could form crystals at this temperature since the T_c of PLA was much higher than the T_m of PCL. Well-defined spherulites of PLA segments could be observed. After prolonged crystallization time at 115 °C, the samples were immediately cooled to 30 °C, only PCL segments could crystallize at this temperature. Generally, if the weight fraction of the blending component is lower than 20%, it will be difficult to crystallize.[51] The crystal morphology was shown in Fig. 5. For PLA/LB-PCLA-15, the spherulites of PLA were integrity which was not influenced by the sporadic and small PCL crystals. The crystals of PCL segments were almost overlapped or confined in the micro-domains of PLA. The size of dispersed PCL crystals increased with adding the LB-PCLA copolymer. The crystallization ability of PCL segments was improved since the volume fraction of LB-PCLA increased. The PCL crystals were located on the vacant position where PLA crystals reserved in advance. The PLA crystals were not gradually covered by the growing PCL crystals. There was an interesting phenomenon that the PCL crystals nucleated and grew confined not only in the inter-spherulite but also intra-spherulite regions of pre-crystallized PLA. It suggested that the phase separation between the PLA and PCL segments was confined to smaller length scales owing to the LB-PCLA copolymer. Different from PLA/LB-PCLA blends, the PCL crystals in the PLA/PCL blends just grew

inside the dark inter-spherulites region of pre-crystallized PLA. The size of PCL crystals was larger than that of PLA/LB-PCLA blends for all the same content (Fig. 6). The prominent phase separation for PLA/PCL blends was observed since the PCL and PLA were typically immiscible biodegradable polymers. This phenomenon was very similar to the formation which occasionally occurs in immiscible crystalline–crystalline blends.[17] The size of PCL crystals for PLA/LB-PCLA-15 was much smaller than other PLA/LB-PCLA blends and PLA/PCL blends, which was considered to be induced by the small amount of LB-PCLA copolymer. The phase separation between PCL segments and PLA matrix was suppressed effectively by the copolymerization and long-chain branched molecular structure.

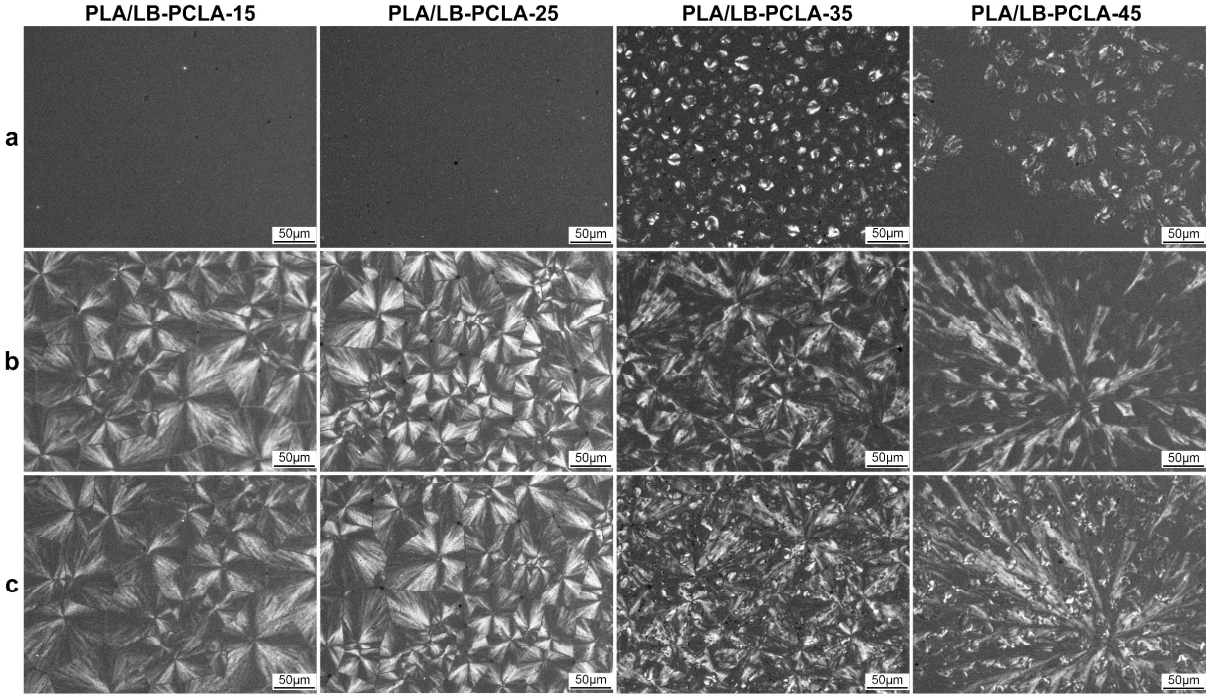

Fig. 5 Polariscope photos of PLA/LB-PCLA blends with different LB-PCLA contents crystallized at 30 °C (a) and 115 °C (b) respectively after being thermally treated at 190 °C for 3 min; crystallized at 30 °C after crystallization at 115 °C (c) The scale bar in all micrographs is 50μm.

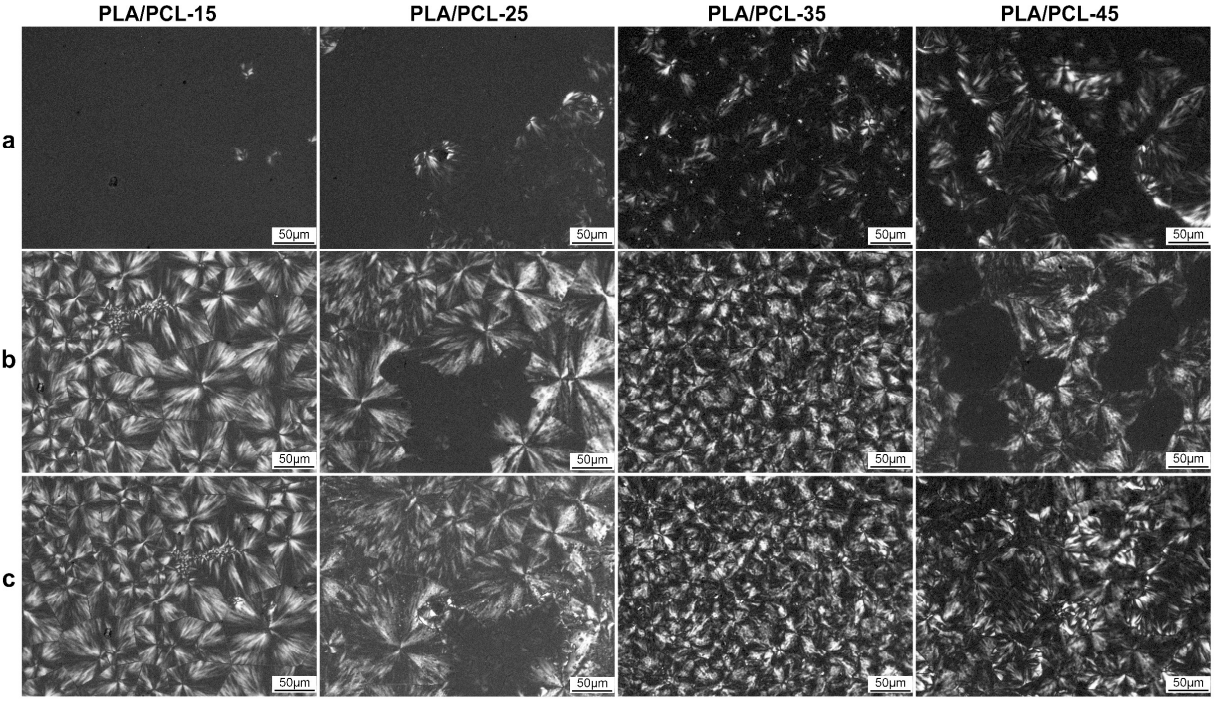

Fig. 6 Polariscope photos of PLA/PCL blends with different PCL contents crystallized at 30 °C (a) and 115 °C (b) respectively after being thermally treated at 190 °C for 3 min; crystallized at 30 °C after crystallization at 115 °C (c) The scale bar in all micrographs is 50μm.

Cite this: DOI: 10.1039/c0xx00000x

www.rsc.org/xxxxxx

ARTICLE TYPE

The growth rate of neat PLA, PLA/LB-PCLA-15 and PLA/LB-PCLA-25 under 115 °C after thermal treated at 190 °C for 3 minutes could be calculated from POM images. The PLA/LB-PCLA-35 and PLA/LB-PCLA-45 were not shown in this figure. Since the larger phase separation caused the complex and irregular crystal morphology, and the spherulite growth rates of these samples cannot be calculated precisely. As shown in Fig. 7. The growth rate of PLA segments in PLA/LB-PCLA-15 at 115 °C was much faster than those of neat PLA and PLA/LB-PCLA-25. The spherulite growth rates were consistent with the isothermal crystallization result that the overall crystallization rate of PLA/LB-PCLA blends was accelerated by a small addition of LB-PCLA copolymer. It suggested that the degree of phase separation and interfacial compatibility had an important influence on PLA crystallization.

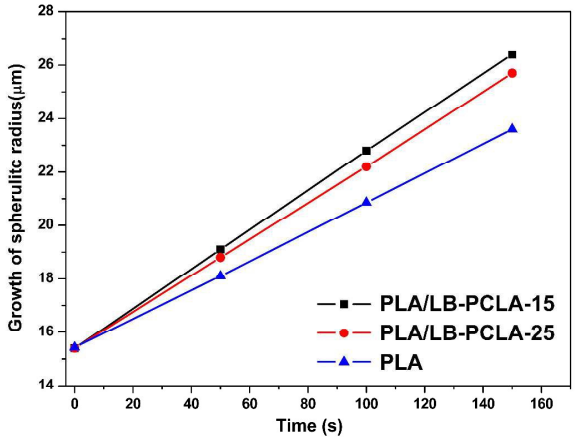

Fig. 7 The growth rate of PLA segments of neat PLA, PLA/LB-PCLA-15 and PLA/LB-PCLA-25 crystallized at 115 °C.

Observing T_g value variation trend to investigate phase separation and compatibility is an effective method.[51] The glass transition of PLA segments of PLA/LB-PCLA blends in DSC curve was overlapped by the melting peak of the PCL segments, and the T_g of PCL was not observed in DSC curve. Therefore, we observed the T_g values of the PLA and PCL segments by Dynamic mechanical analysis (DMA) since the mechanisms of two test methods are different. Fig. 8 showed the tan delta as a function of temperature for neat PLA and PLA/LB-PCLA blends.

Obviously, two relaxation peaks could be observed on the tan delta plots. Compared to other PLA/LB-PCLA blends, the relaxation peak of PLA/LB-PCLA-15 at the low temperature region turned to be broader and less prominent, even almost disappeared. Here we introduced the ΔT_g, which is the difference between the T_g's of the PCL and PLA phases, for evaluating the compatibility. The ΔT_g value of PLA/LB-PCLA-15 was smaller than other blends, suggested that this sample had better interfacial compatibility and smaller phase separation than other blends owing to the copolymerization of PCL and PLA. With increasing LB-PCLA content, the value of ΔT_g was increased. It suggested that the two polymers of PLA and LB-PCLA are less compatible. Meanwhile, the ΔT_g value of PLA/PCL blends was all larger than PLA/LB-PCLA blends and independent of composition, which ascribe to the thermodynamic incompatibility between PLA and PCL. The octopus-like long chain branched molecular structure of LB-PCLA is also in favor of the compatibility between PCL and PLA since this special structure may increase the intermolecular interaction and chain entanglement, resulted in tight adherence between PCL phase and PLA matrix. However, with increase of LB-PCLA content, the cohesion of PCL segments were also increased and resulted in obvious phase separation.

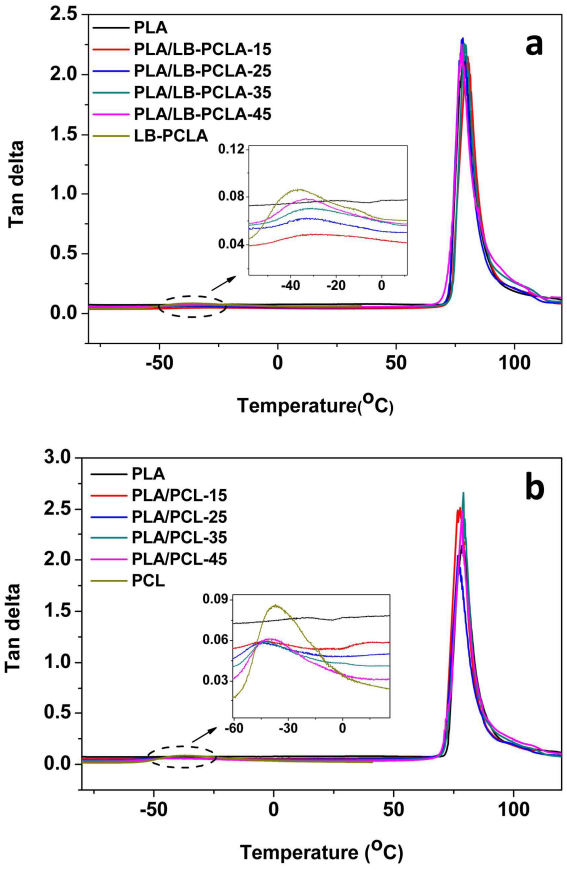

Fig. 8 Temperature dependence of tan delta for PLA/LB-PCLA blends and PLA/PCL blends.

It is well known that the properties of polymer blends are strongly dependent on their phase morphology and particle size. The TEM analysis was further employed to observe the morphological structure of PLA/LB-PCLA blends and PLA/PCL blends. Fig. 9 showed the TEM micrographs of the blends.

Table 3 Detailed DMA data of PLA/LB-PCLA and PLA/PCL blends.

Sample	T_g(PLA) (°C)	T_g(PCL) (°C)	ΔT_g (°C)
PLA	79.2	-	-
PLA/LB-PCLA-15	77.6	-23.1	100.7
PLA/LB-PCLA-25	77.9	-31.8	109.7
PLA/LB-PCLA-35	78.4	-32.5	110.7
PLA/LB-PCLA-45	79.1	-33.3	112.4
LB-PCLA	-	-37.9	-
PLA/PCL-15	77.5	-43.9	121.4
PLA/PCL-25	76.7	-44.3	121.0
PLA/PCL-35	78.3	-43.6	121.9
PLA/PCL-45	79.2	-41.0	120.2
PCL	-	-37.5	-

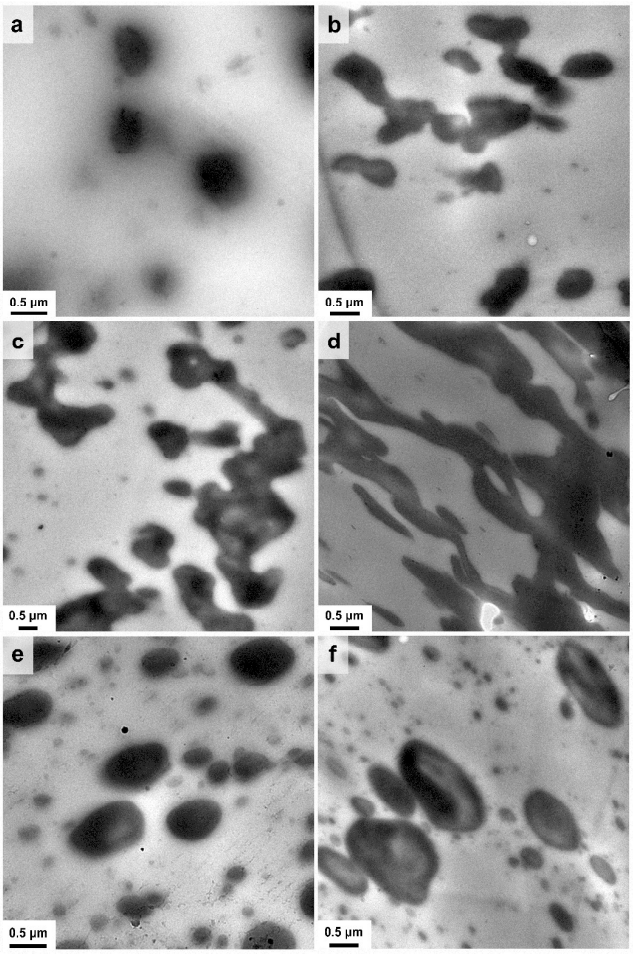

Fig. 9 TEM images of (a) PLA/LB-PCLA-15 (b) PLA/LB-PCLA-25 (c) PLA/LB-PCLA-35 (d) PLA/LB-PCLA-45 (e) PLA/PCL-15. (f) PLA/PCL-25

The phase morphology was observed for all the PLA/LB-PCLA blends as evidenced by the dark subdomains in the PLA matrix. The dark subdomains were formed by aggregation of LB-PCLA copolymer while the light subdomains were PLA segments, since LB-PCLA copolymer was selectively stained more easily than PLA matrix. As expected that phase separation occurred for all PLA/LB-PCLA blends. As shown in Fig. 9a, typical well diffused droplet-in-matrix structure was observed for PLA/LB-PCLA-15. With increase of LB-PCLA content, the dispersed droplets gradually aggregated and were more difficult to be distinguished. Moreover, the shape of PCL phase in the PLA matrix became irregular rather than typical ellipse shape. The blends even exhibited quasi continuous phase separation when LB-PCLA content was 35% and bicontinuous phase separation when LB-PCLA content was 45%. This phenomenon is quite different from PLA/PCL blends. As shown in Fig. 9e and 9f, the PLA/PCL-15 and PLA/PCL-25 blends, which has similar content of PCL segments as PLA/LB-PCLA-25 and PLA/LB-PCLA-45, respectively, still exhibited droplet-in-matrix structure with typical ellipse shape. The domain size of PCL were 0.76μm, 0.89μm for PLA/PCL-15, PLA/PCL-25, respectively. This result suggested that there was good interfacial compatibility between the PCL and PLA phases in PLA/LB-PCLA blends than those of PLA/PCL blends. Therefore, the long-chain branched structure of copolymer at interface would increase the compatibility between two phases. Phase diagram of binary blends obey the Flory-Huggins theory.[52] The PLA/LB-PCLA blends could be ascribed to a UCST blend and the structural differences exhibited in Fig. 9 are due to different kinetics, based on different positions on the phase diagram. PLA/LB-PCLA-15 is close to the bimodal curve, it showed droplet-like structure in the metastable region which indicated that they have a nucleation and growth mechanism. Meanwhile, the bicontinuous structures of PLA/LB-PCLA blends with copolymer content higher than 25% suggest a spinodal decomposition-like mechanism common to blends deep within the two-phase region.

Mechanical properties and tensile fracture surfaces

Mechanical properties of polymer blends depended largely on the resulting particles size and morphology. It was accepted that phase separation with small size was necessary in toughed PLA systems. If the size of particle was too large, they would initiate unstable cracks.[53] The significant increase in toughness was also attributed to the morphology induced by the effective interfacial interaction in the polymer blends.

The tensile strength and elongation at break of neat PLA and PLA/LB-PCLA blends were investigated by a tensile test. Neat PLA showed a typical curve of brittle fracture with the elongation at break, tensile strength, of 7.8%, 57.7 MPa, respectively, while PLA/LB-PCLA blend exhibited characteristic nature of ductile fracture with apparent yielding occurred in the stress−strain curves. Fig. 10 showed the stress–strain curves of neat PLA and PLA/LB-PCLA blends. The detailed data was shown in Table 4. The tensile test of PLA/LB-PCLA blends containing 5wt% of LB-PCLA copolymer was also performed. However, the elongation at break of this sample was as small as neat PLA. It indicated that a small amount of the LB-PCLA copolymer did not toughen the PLA matrix, so this sample was not mentioned again in this work. The PLA/LB-PCLA-15 showed the maximum elongation at break, 210%, an increase of 30 times compared with that of neat PLA. Moreover, the tensile strength decreased not too much. However, with increase of LB-PCLA content, the elongation at break decreased. This result suggested that the toughened effect of LB-PCLA on PLA matrix is directly depending on its content. LB-PCLA copolymer played the pronounced toughened effect at low content. It could be attributed to the strong interfacial interaction between PCL phase and PLA matrix at low content. The tensile strength of PLA/LB-PCLA

blends was lower than that of neat PLA owing to the increased toughened effect. A similar phenomenon was also reported in neat PLA or other polymer blends.[53]

To verify the morphology of LB-PCLA copolymer in the PLA/LB-PCLA blends which is an important factor for blends' physical properties, the detailed tensile fracture surfaces of the blends were studied by SEM.

Table 4 Mechanical properties of PLA/LB-PCLA blends and PLA/PCL blends.

Sample	Tensile strength (MPa)	Elongation at break (%)
PLA	57.7±2.7	7.1±0.9
PLA/LB-PCLA-15	46.7±0.4	210.7±8.5
PLA/PCL-15	48.4±0.5	71.5±6.5
PLA/LB-PCLA-25	42.5±0.4	62.4±2.1
PLA/PCL-25	40.5±0.4	9.9±4.4
PLA/LB-PCLA-35	32.8±0.1	40.8±7.5
PLA/PCL-35	31.8±0.3	4.7±2.4
PLA/LB-PCLA-45	30.6±3.6	22.6±1.8
PLA/PCL-45	29.4±2.4	5.5±1.6

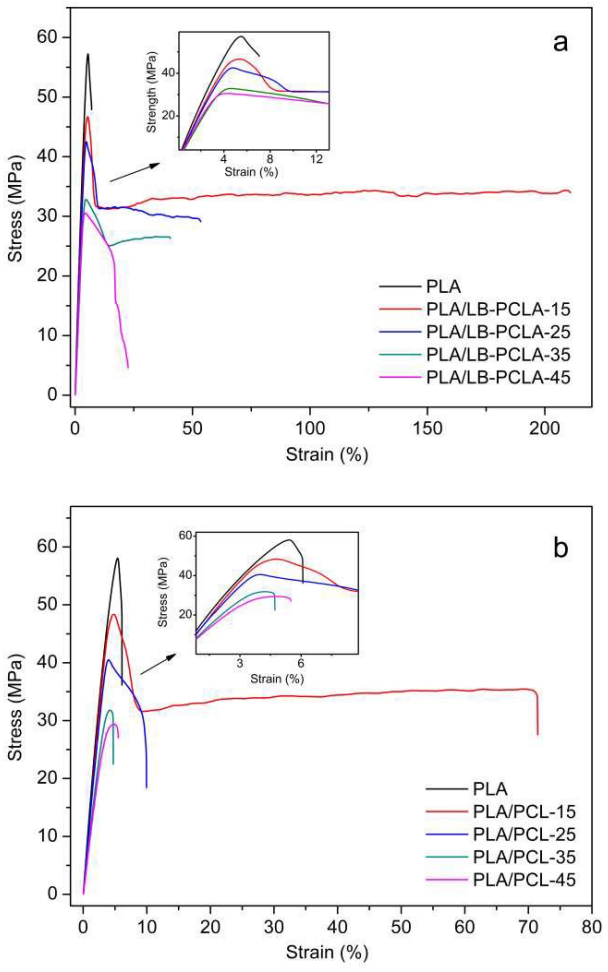

Fig. 10 Stress–strain curves of PLA/LB-PCLA and PLA/PCL blends.

Fig. 11 presented the SEM micrographs of tensile fracture surfaces of PLA/LB-PCLA blends. As shown in the graphs, Neat PLA showed a typical brittle fracture, and the tensile fracture surface of neat PLA was very smooth without any phase separation, while the surfaces were rougher and more prominent deformation for all PLA/LB-PCLA blends. This phenomenon suggested PLA/LB-PCLA blends were ductile fracture. In this case, the terminal PLA group of long-chain branched structure LB-PCLA copolymer worked as toughening to initiate serious stress yielding to PLA matrix. Especially for LB-PCLA-15, many long fibrils existed in the tensile fracture surfaces, suggested that there was sufficient interfacial interaction between the PLA and LB-PCLA, which was consistent with the results that we discussed above. Compared to PLA/LB-PCLA-15, all the other blends presented short and coarse fibrils, which were correspondent to the mechanical properties of PLA/LB-PCLA blends properties observed by tensile measurement.

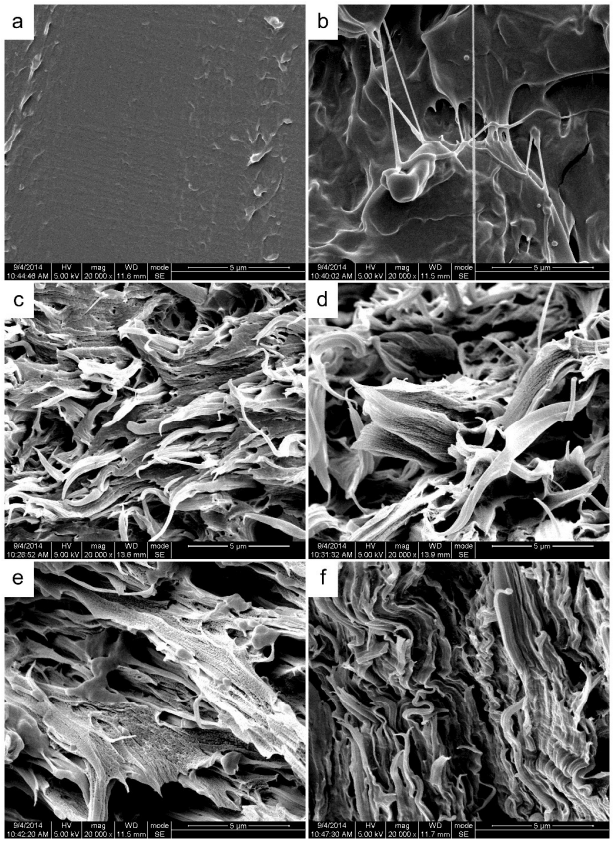

Fig. 11 SEM micrographs for the tensile fracture surfaces of PLA/LB-PCLA blends. (a) neat PLA (b) PLA/LB-PCLA-15(c) PLA/LB-PCLA-25 (d) PLA/LB-PCLA-35 (e) PLA/LB-PCLA-45 (f) LB-PCLA.

Melt rheological behaviour

In order to investigate the effect of the long-chain branched structure copolymer on the chain mobility of PLA, the melt rheological behaviour was studied by a rheometer.

Fig. 12 showed the complex viscosities of the neat PLA, LB-PCLA, PLA/LB-PCLA-15, neat PCL and PLA/PCL-15 with oscillatory frequency. From this figure, it was readily apparent that the long-chain branched structure had a significant influence on the complex viscosity at lower frequency. Neat PLA, neat PCL and PLA/PCL-15 were all exhibited obvious Newtonian-plateau. No obvious Newtonian-plateau was observed for LB-PCLA and PLA/LB-PCLA-15 which could be attributed to the

branched structure of LB-PCLA copolymer. Moreover, the shear thinning of LB-PCLA and PLA/LB-PCLA-15 started at lower frequency than that of neat PLA. The branched structure could form sufficient entanglements between PLA matrix and LB-PCLA copolymer. It was resulted longer relaxation time which could make molecules orientation enough to reduce the viscosity of PLA matrix. Therefore, PLA/LB-PCLA-15 exhibited a higher complex viscosity than those of neat PLA and PLA/PCL-15 with similar molecular weight. While at high frequency, the PLA/LB-PCLA-15 exhibited a lower viscosity than that of neat PLA owning to a higher degree of shear thinning. It suggested that the processability of PLA was appropriately improved. The complex viscosity of LB-PCLA and PLA/LB-PCLA-15 were nearly equal. The rheological response of the system is controlled by the polymer matrix in the high frequency region (>100 rad/s). The viscosities of all samples could be fitted by the Cross equation [54] given by Eqn.(8).

$$\eta^*(\omega) = \frac{\eta_0}{1+(\lambda\omega)^n} \quad (8)$$

Where λ is relaxation time, η_0 is zero-shear viscosity, and n is shear-thinning index, which indicates the degree of non-Newtonian behaviour. The detailed data were shown in Table 5.

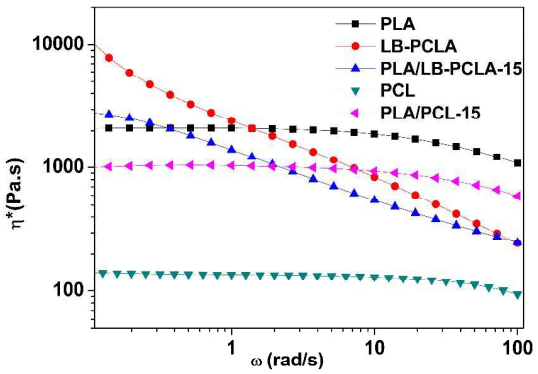

Fig. 12 Complex viscosities versus angle frequency of the neat PLA, LB-PCLA, PLA/LB-PCLA-15, PCL and PLA/PCL-15 at 190 °C.

As shown in Table 5, the LB-PCLA exhibited the most obvious non-Newtonian behaviour. The long-chain branched structure was the main reason for such results. The long-chain branched structure of the copolymer also have important influence on the rheological behavior of the PLA/LB-PCLA blend. The zero-shear viscosity and relaxation time of PLA/LB-PCLA-15 are higher than that of PLA/PCL-15. Similar phenomena were also observed for other long-chain branched structure polymers.[44]

The Storage (G') and loss (G") moduli for the neat PLA, PLA/LB-PCLA-15 and PLA/PCL-15 were shown in Fig. 13. The G' and G" increased with increasing ω. In the low frequency region, neat PLA and PLA/PCL-15 showed typical terminal behaviour, following the scaling relations G' ∝ ω^2 and G" ∝ ω. The slope of the PLA/LB-PCLA-15 which was calculated by computer decreased compared to those of neat PLA and PLA/PCL-15 owing to the long relaxation time caused by the LB structure of PLA/LB-PCLA-15. Moreover, the value of the G' and G" for PLA/LB-PCLA-15 were very close to each other. It indicated that the three-dimensional network-like formation of LB-PCLA played a predominant role in the viscoelastic behaviour of the system.

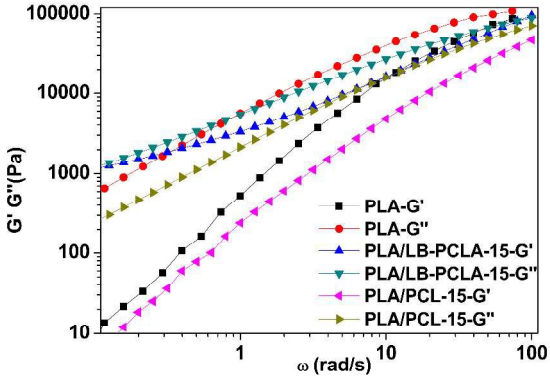

Fig. 13 Storage modulus and loss modulus versus angle frequency curves of the neat PLA and PLA/LB-PCLA-15 and PLA/PCL-15 at 190 °C.

Table 5 Rheological characteristics of neat PLA, LB-PCLA, PLA/LB-PCLA-15, PCL and PLA/PCL-15.

Sample	η_0 (Pa.s)	λ (s)	n
PLA	2086	0.01	1.22
LB-PCLA	11258	5.97	0.61
PLA/LB-PCLA-15	2834	0.57	0.71
PCL	202	0.0019	1.23
PLA/PCL-15	991	0.0040	0.73

Conclusions

Long-chain branched copolymer (LB-PCLA) has been successfully synthesized via the reaction between the terminated group PLA-OH and PCL-3OH precursors using HDI as the chain-extending agent. The crystalline temperature T_c of PLA segments decreases and the relative crystallinity χ_c and crystallization rates increase evidently with adding LB-PCLA copolymer, but the crystal structure has not been disturbed according to the results investigated by WAXD technique. The copolymerization and long-chain branched molecular structure of LB-PCLA copolymer are in favor of the interfacial compatibility between PCL phase and PLA matrix. The tensile toughness of PLA was improved significantly through LB-PCLA copolymer with small content. The elongation at break for PLA/LB-PCLA-15 was improved to more than 30 times than that of neat PLA. Meanwhile, the stress was balanced at a good level. Small-amplitude oscillatory shear experiments showed that the LB structure has obvious influence on the rheological behaviour of PLA blends. For PLA/LB-PCLA-15, zero-shear viscosity η_0, the Storage (G'), loss (G") moduli, relaxation time λ and shear-thinning index n increase at low frequency, which are in accordance with those of representative LB polymers. Therefore, the rheological behaviour of PLA could be well-controlled via blending with the LB copolymer. In summary, the optimal concentration of LB-PCLA copolymer, 15%, is relatively low and

represents a commercial cost benefit since copolymers are more expensive to produce than homopolymers. We developed a comprehensive solution strategy to toughen PLA without injuring other properties such as tensile strength, crystallization and rheological behaviour.

Acknowledgments

This work was financially supported by the National Natural Science Foundation of China (No. 21474066 and 51421061), and State Key Laboratory of Polymer Materials Engineering (No. sklpme2014-3-09). The Analytical and Testing Center of Sichuan University provided TEM analysis.

Notes and references

National Engineering Laboratory of Eco-Friendly Polymeric Materials (Sichuan), State Key Laboratory of Polymer Materials Engineering, College of Chemistry, Sichuan University, Chengdu, 610064, China. E-mail: chensichong@scu.edu.cn, kkyangscu@126.com.

1 L. Fambri, A. Pegoretti, R. Fenner, S. D. Incardona and C. Migliarisi, *Polymer*, 1997, **38**, 79-85.
2 S. Saeidlou, M. A. Huneault, H. B. Li and C. B. Park, *Progress in polymer science,* 2012, **37**, 1657-77.
3 Z. G. Wang, L. Q. Yu, M. M. Ding, H. Tan and J. H. Lia, *Polym Chem.,* 2011, **2**, 601–607.
4 H. Z. Liu and W. J. Song, *Macromolecules,* 2011, **44**, 1513-1522.
5 B. Meng and J. J. Deng, *European Polymer Journal*., 2012, **48,** 127-135.
6 J. H. Yang, S. H. Lin and Y. D. Lee, *J Mater Chem.,* 2012, **22**, 10805–10815.
7 C. Choochottiros, I. J. Chin, *Eur Polym.,* 2012, **49**, 957-966.
8 W. Chumeka, P. Pasetto, J. F. Pilard and V. Tanrattanakul, *Polymer,* 2014, **55**, 4478-4487.
9 P. A. Delgadoa, M. A. Hillmyer, *RSC Adv.*, 2014, **4**, 13266-13273.
10 J. S. Qiu, C. Y. Xing, X. J. Cao, H. T. Wang, L. Wang and L. P. Zhao, *Macromolecules*, 2013, **46**, 5806–5814.
11 E. T. H. Vink, K. R. Rabago, D. A. Glassner and P. R. Gruber, *Polym Degrad and Stabil.,* 2003, **80**, 403-419.
12 A. Södergård, M. Stolt, *Prog Polym Sci.,* 2002, **27**, 1123-1163.
13 M. E. Broz, D. L. VanderHart and N. R. Washburn, *Biomaterials,* 2003, **24**, 4181-4190.
14 S. H. Lee, S. H. Kim and Y. K. Han, *Polym Chem.,* 2002, **40**, 2545-2555.
15 R. Bhardwaj and A. K. Mohanty, *Biomacromolecules,* 2007, **8**, 2476-2484.
16 Y. S. He, J. B. Zeng, G. C. Liu and Y. Z. Wang, *RSC Adv.* 2014, **4**, 12857-12866.
17 Y. Q. Zhang, Z. K. Wang, F. Jiang, J. Bai and Z. G. Wang, *Soft Matter,* 2013, **9**, 5771-5778.
18 S. Aslan, L. Calandrelli, P. Laurienzo, M. Malinconico and C. Migliaresi, *J Mater Sci.,* 2000, **35**, 1615-1622.
19 C. H. Kim, K. Y. Cho, E. J. Choi and J. K. Park, *J Appl Polym Sci.,* 2000, **77**, 226-231.
20 H. B. Li and A. Michel, *Polymer,* 2007, **48**, 6855-6866.
21 J. Odent, P. Leclere, J. M. Raquez and P. Dubois, *Eur Polym. J.*, 2013, **49**, 914-922.
22 L. J. Han, C. Y. Han and L. S. Dong, *Polym Int*., 2013, **62**, 195-303.
23 P. Ma, A. B. Spoelstra, P. Schmit and P. J. Lemstra, *Eur Polym*., 2013, **49**, 1523-1531.
24 X. Li, H. L. Kang, J. X. Shen, L. Q. Zhang, T. Nishi and K. Ito, *Polymer*, 2014, **55**, 4313-4323.
25 I. Lee, T. R. Panthani and F. S. Bates, *Macromolecules,* 2013, **46**, 7387-7398.
26 T. Hideto and T. Hiroki, *Polymer,* 2006, **47**, 3826-3837.
27 Z. H. Xu and Y. H. Niu, *Polymer,* 2010, **51**, 730-737.
28 J. R. Dorgan and J. S. Williams, *J Rheol*., 1999, **49**, 1141-1155.
29 J. Y. Liu, S. J. Zhang, L. Y. Zhang and Y. Q. Bai, *Polymer,* 2014, **55**, 2472-2480.
30 N. Othman, C. L. Xu, P. Mehrkhodavandi and S. G. Hatzikiriakos, *Polymer,* 2012, **53**, 2443-2452.
31 L. V. Palade and H. J. Lehermeier, *Macromolecules*, 2001, **34**, 1384-1390.
32 M. G. McKee, S. Unal, G. L. Wilkes and T. E. Long, *Prog Polym Sci*., 2005, **30**, 507-539.
33 H. G. Fang, Y. Q. Zhang, J. Bai and Z. G. Wang, *Macromolecules*, 2013, **46**, 6555-6565.
34 M. Pitsikalis, S. Pispas, J. W. Mays and N. Hadjichristidis, *Adv Polym Sci.,* 1998, **135**, 1-137.
35 A. M. Fischer, F. K. Wolf and H. Frey, *Macromolecular chemistry and physics,* 2012, **213**, 1349-1358.
36 S. Kurzbeck, F. Oster and H. Münstedt, *J Rheol*., 1999, **43**, 359-374.
37 D. J. A. Cameron and M. P. Shaver, *Chem Soc Rev.,* 2011, **40**, 1761-1776.
38 L. Jiang, M. P. Wolcott and J. W. Zhang, *Biomacromolecules,* 2006, **7**, 199-207.
39 M. L. Robertson, K. Chang, W. M. Gramlich and M. A. Hillmyer, *Macromolecules*, 2010, **43**, 1807-1814.
40 W. M. Gramlich, M. L. Robertson and M. A. Hillmyer, *Macromolecules,* 2010, **43**, 2313-2321.
41 C. H. Ho, C. H. Wang, C. I. Lin and Y. D. Lee, *Polymer,* 2008, **49**, 3902-3910.
42 H. T. Oyama and T. Inoue, *Macromolecules,* 2001, **34**, 3331-3338.
43 D. F. Wu, Y. S. Zhang and W. Yu, *Biomacromolecules*, 2009, **10**, 417-424.
44 F. Chen, S. C. Chen, K. K. Yang, X. L. Wang and Y. Z. Wang, *Eur Polym*., 2010, **46**, 24-33.
45 L. X. Zeng, M. J. Liu, S. C. Chen and Y. Z. Wang, *Polym Chem*., 2012, **3**, 2537-2544.
46 Z. H. Xu and Y. H. Niu, *Polymer,* 2010, **51**, 730-737.
47 A. J. Oshinski, H. Keskkula and D. R. Paul, *Polymer,* 1996, **37**, 4891-4907.
48 M. Avrami, *J Phys Chem*., 1939, **7**, 1103-1112.
49 M. Avrami, *J Phys Chem*., 1940, **8**, 212-224.
50 V. Ojijio, T. Malwela, S. S. Ray and R. Sadiku, *Polymer*, 2012, **53**, 505-518.
51 C. Cai, L. Wang and C. M. Dong, *Polym Chem*., 2006, **44**, 2034-2044.
52 J. H. Lee, M. L. Ruegg, N. P. Balsara, Y.Q. Zhu and M. H. Kim, *Macromolecules,* 2003, **36**, 6537-6548.
53 H. Z. Liu, F. Chen, B. Liu, G. Estep and J. W. Zhang, *Macromolecules,* 2010, **43**, 6058-6066.
54 M. M. Cross, *J Colloid Sci.,* 1965, **20**, 417-437.